Power Electronics and Drives
Volume 11(46), 2026 DOI: 10.2478/pead-2026-0004

Hybrid Type-2 Fuzzy Logic–Extended Kalman Filter Approach for ITSC Fault Detection in PMSM Drives for Electric Vehicles

Research Paper

Mabrouka Romdhane[1], Mohamed Naoui[2,*], Abdelmalek Gacem[3], Ali Mansouri[1,4]

[1]*Research Laboratory Technology Energy and Innovative Materials, Faculty of Sciences of Gafsa, Gafsa, Tunisia*
[2]*Research Unit of Processes Energy Environment and Electrical System, National Engineering School of Gabes, Gabes, Tunisia*
[3]*LGEERE Laboratory Department of Electrical Engineering, University of El-Oued, El-Oued, Algeria*
[4]*Higher School of Applied Sciences and Technology of Gafsa Department of Industrial Systems, University of Gafsa, Gafsa, Tunisia*

Received: 09 December, 2025; Received in the revised form: 02 February, 2026; Accepted: 08 February, 2026

Abstract: The detection of Inter-Turn Short Circuit (ITSC) in electrical machines is a critical operation, particularly in electric vehicle (EV) motor drives. In this paper, a hybrid approach of type-2 fuzzy logic (T2-FL) and extended Kalman filter (EKF) is proposed in order to detect ITSC fault in the permanent magnet synchronous motor (PMSM) released by MATLAB/SIMULINK. The PMSM stator resistance is estimated through T2-FL, while the motor current, rotor speed and rotor angular are estimated by the EKF, taking advantage of its dynamic features. The results under high value and poor visibility of the ITSC resistance fault show that the root mean square error (RMSE) of the fault current is 0.2303. Moreover, comparison of the type-2 fuzzy logic and extended Kalman filter (T2-FL–EKF) strategy with the conventional EKF and fuzzy logic–extended Kalman filter (FL–EKF) approaches showed a significant optimisation in both speed control and ITSC fault detection.

Keywords: *electric vehicle • permanent magnet synchronous motor • type-2 fuzzy logic • extended Kalman filter • inter-turn short circuit*

1. Introduction

The integration of artificial intelligence (AI) in electric vehicles (EVs) is now a key driver to promote safer, more reliable and better performance of the EV. This integration includes navigation and autonomous driving (Miller et al., 2024; Tan et al., 2024), power strategies and energy management (Arévalo et al., 2024; Huang et al., 2025), regenerative braking and risk assessment (Cavus et al., 2025; Prakash, 2025). Inter-turn short circuit (ITSC) is one of the key risk factors in the motor drive safety of the EV (Hang et al., 2024). This electrical fault affects electrical machines such as the permanent magnet synchronous motor (PMSM), which are one of the first candidates in the EV industry for their accounting in terms of power productivity, financial constraints and operating conditions (Zhang et al., 2025).

To address these challenges, computational advanced techniques, specifically artificial neural networks (ANNs), fuzzy logic (FL) methodologies and hybrid computational intelligent control algorithms with machine learning and deep learning, offer new means for advanced condition monitoring and early fault detection (Lang et al., 2022). Building upon classic FL, type-2 fuzzy logic (T2-FL) offers several advantages, notably a better ability to handle high uncertainties in estimating highly variable parameters. In an interval type-2 fuzzy set, the footprint of uncertainty (FOU) is the region that visually represents the ambiguity or imprecision of the fuzzy

* *Email: mednaouiing@yahoo.com*

membership function. It is a shaded region with a top edge called the upper function and a bottom edge defined as the lower function. This structure allows for the simultaneous modelling of uncertainty related to the input data and uncertainty affecting membership degree, which enables it to more accurately represent a non-linear, noisy or poorly modelled system (De et al., 2022). In this context, Dilimi et al. (2021) propose an advanced control method for active fault tolerance of a BLDC motor by combining the T2-FL command and a higher order sliding mode control, which improves both steady-state performance and the system's dynamic response, besides phase current monitoring and fault diagnosis (Nguyen et al., 2025). Ladjal et al. (2022) introduce a new approach for implementing fault-tolerant strategy control in a dual three-phase induction machine that implements T2-FL and integrates an adaptive control law to manage malfunctions due to rotor bar breakage in a squirrel cage machine (Nesri et al., 2024).

Recently, Zeng et al. (2025) used T2-FL technology for managing the hydropower system by integrating it with Digital Twin Technology-Neural networks. This system consists of wind turbines and a doubly fed induction generator. The exploitation of T2-FL mitigates inherent uncertainties and inaccuracies, and enables real-time monitoring and predictive analysis. The neural networks then refine these predictions using historical and real-time data. This approach resulted in an 11.48% improvement in the overall system performance.

Within the same concept of uncertainty and perturbation in real systems, Jahanshahi et al. (2022) present an overview of the modelling and implementation of T2-FL that can be applied in the control of different systems of integer and fractional order. The authors here show some studies that have compared T2-FL with T1-FL (Sanchez et al., 2015; Castillo et al., 2016) and that have proven that T2-FL systems are the best choice for problems exhibiting a high degree of uncertainty.

Furthermore, in hybrid AI methods in fault detection, an architecture for multilayer ANNs trained via back propagation has been detailed in Lazar et al. (2021) for detecting and isolating ITSC fault in induction motor base, where the approach uses monitoring of the instantaneous average power, measured from stator currents and voltages, to identify the ITSC fault. In Shao et al. (2020), a deep learning methodology is utilised by the authors for induction motor fault diagnosis, leveraging a convolutional neural network (CNN) architecture capable of automatically learning discriminating representations from time frequency images obtained by transforming sensor signals into wavelets. Nyanteh et al. (2013) combined the extended Kalman filter (EKF) with ANNs and Particle Swarm Optimization (PSO) to detect fault characteristics. In Ertargin et al. (2024), a hybrid CNN-LSTM (long short-term memory) developed with deep learning model is proposed to detect the mechanical and electrical faults in electric motors from three different accelerometer sensor configurations. The EKF has proven particularly effective for estimating system states and identifying parameter variations associated with faults (Isermann, 2004); besides, Namdar et al. (2022) and Ouamara et al. (2023) confirmed EKF's reliability in identifying ITSC fault in induction motors.

Considering that the ITSC fault contributes to a progressive degradation of torque and overheating of the windings, which provides uncertainty and noise on the stator resistance measurement and in extreme cases, a complete failure of the propulsion system, we proposed in our previous method (Romdhane et al., 2023), an approach that unites the EKF's analytical precision with the conventional FL to approximate the stator resistance and detect ITSC fault. Nevertheless, these approaches show uncertainties in estimation under demanding operating conditions. In particular, the detection of initial ITSC faults is characterised by a weak signature or low visibility, which exhibits insufficient reliability when the defect is subtle, leading to critical non-detections. Based on this model and the theoretical background study, we are motivated in this work to upgrade the previous fuzzy logic–extended Kalman filter (FL–EKF) model to a hybrid type-2 fuzzy logic and extended Kalman filter (T2-FL–EKF).

The main objective of the proposed approach is the development of a robust detection algorithm for ITSC fault in PMSM with high sensitivity even in low-visibility conditions, which is one of the limits of the mentioned existence methods. This approach demonstrates an effective stabilisation in the stator resistance estimation under high uncertainties, as quantitatively proven.

This work is presented as follows: a description of the healthy and defective PMSM mathematical models is presented in Section 2. Section 3 details the hybrid T2-FL–EKF proposed approach. The results obtained from the simulated model are presented in Section 4, carried out by a quantitative analysis. Section 5 highlights the improvement attained by the proposed method and the upcoming experimental projections.

2. Mathematical Machine Model

2.1. PMSM model

The mathematical representation of PMSM in the *dq* reference frame is a required phase for the implementation of the vector control for model simulation through MATLAB/SIMULINK. The projection of the stator variables onto the orthogonal axis leads to separating the flux control *d*-axis from the electromagnetic torque *q*-axis. In this frame, the motor equations are expressed as follows:

$$\begin{cases} V_d = R_s i_d + L_d \dfrac{di_d}{dt} - \omega_e L_q i_q \\ V_q = R_s i_q + L_q \dfrac{di_q}{dt} + \omega_e \left(L_d i_d + \psi_f \right) \end{cases} \tag{1}$$

- V_d and V_q: Stator voltages;
- i_d and i_q: Stator currents;
- R_s: Stator resistance (0.44 Ω);
- L_d and L_q: *d*-*q* axis inductances (0.0031 H);
- ω_e: Electrical angular speed;
- ψ_f: Flux linkage produced by the permanent magnets (0.124 Wb).

The PMSM's generated electromagnetic torque is determined by the following expression:

$$T_e = \frac{3}{2} \rho \left(\psi_f i_q + (L_d - L_q) i_d i_q \right) \tag{2}$$

In which ρ denotes the four pole pairs of the PMSM.
The mechanical dynamics of the rotor are governed by:

$$J \frac{d\omega}{dt} + B\omega_m = T_e + T_l \tag{3}$$

Where, J, B, ω_m and T_l are, respectively, J: Rotor's moment of inertia (0.0002 kg/m^2), B: Viscous friction coefficient, ω_m: Mechanical angular speed, T_l: Load torque

2.2. Proposed PMSM fault model

The machine analysed in this study is characterised by the following:

- Surface permanent magnet (SPM) motor;
- Integral-slot concentrated winding;
- Three-wire Y configuration.

The conventional way to model an ITSC fault is by introducing a resistance R_f that represents the fault as it is illustrated in Figure 1 (Romdhane et al., 2023).

The stator phase is divided into a healthy portion a_1 and a faulty portion a_2, while the fault resistance R_f is connected in parallel with a_2 (Liu et al., 2023; Yu et al., 2025).

The electrical representation of the faulty PMSM is described by the following equation (Amiri Ahouee and Mola, 2020):

$$\mathrm{V}_{\mathrm{ITSC}} = R_{\mathrm{ITSC}} \cdot I_{\mathrm{ITSC}} + L_{\mathrm{ITSC}} \cdot \frac{dI_{\mathrm{ITSC}}}{dt} + e_{\mathrm{ITSC}} \tag{4}$$

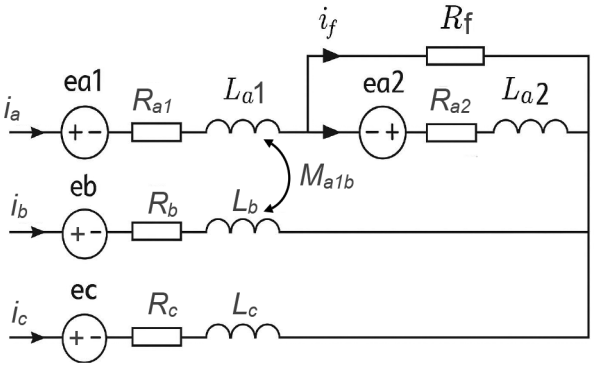

Figure 1. Faulty phase equivalent circuit.

The following parameters are expressed in the (*a*, *b*, *c*) three-phase reference frame, where:

V_{a_ITSC}, V_{b_ITSC}, V_{c_ITSC}: Stator voltages, I_{a_ITSC}, I_{b_ITSC}, I_{c_ITSC}: Stator currents; I_{f_ITSC}: Fault current, L_{ITSC}: Mutual inductance and e_{a_ITSC}, e_{b_ITSC}, e_{c_ITSC}: back electromotive EMF.

Where:

$$\begin{cases} V_{\mathrm{ITSC}} = \begin{bmatrix} V_{a\_\mathrm{ITSC}} & V_{b\_\mathrm{ITSC}} & V_{c\_\mathrm{ITSC}} & 0 \end{bmatrix} \\ R_{ITSC} = \begin{bmatrix} R_s & 0 & 0 & -R_{a_2} \\ 0 & R_s & 0 & 0 \\ 0 & 0 & R_s & 0 \\ -R_{a_2} & 0 & 0 & R_{a_2}+R_f \end{bmatrix} \\ I_{ITSC} = \begin{bmatrix} I_{a\_ITSC} & I_{b\_ITSC} & I_{c\_ITSC} & I_{f\_ITSC} \end{bmatrix} \\ L_{ITSC} = \begin{bmatrix} L_s & 0 & 0 & -L_{a_s}-M_{a_1a_2} \\ 0 & L_s & 0 & -M_{a_2b} \\ 0 & 0 & L_s & -M_{a_2b} \\ -(L_{a_s}+M_{a_1a_2}-M_{a_2b}) & 0 & 0 & L_{a_2} \end{bmatrix} \end{cases} \tag{5}$$

With:

$$\begin{cases} e_{\mathrm{ITSC}} = \begin{bmatrix} e_{a\_\mathrm{ITSC}} \\ e_{b\_\mathrm{ITSC}} \\ e_{c\_\mathrm{ITSC}} \\ -e_{a_2} \end{bmatrix} \\ R_{a_1} = \left(1 - \dfrac{T_{\mathrm{fault}}}{T_{\mathrm{total}}}\right) \cdot R_s \\ R_{a_2} = \dfrac{T_{\mathrm{fault}}}{T_{\mathrm{total}}} \cdot R_s \end{cases} \tag{6}$$

The resistance of the healthy portion of the phase is presented by R_{a_1} while the resistance of the inter-turn circuited portion is represented by R_{a_2} and T_{fault} and T_{total} are, respectively, the number of shorted turns in the sub-winding and the total number of turns per phase.

Using the ratio of these parameters, we can define the ITSC coefficient as follows:

$$\mu = \frac{T_{\mathrm{fault}}}{T_{\mathrm{total}}} \tag{7}$$

The formulation of the torque and its associated mechanical dynamics in the *dq*-axis frame is as follows:

$$\begin{cases} T_e = \frac{3}{2} p\left(\psi_d i_q - \psi_q i_d\right) \\ J\frac{d\omega_r}{dt} + f_r\omega_r + T_{\text{load}} = T_e \end{cases} \tag{8}$$

Here, ω_r: Rotor angular velocity, f_r: Friction coefficient (0.0812 N.m.s./rad).

The following equation is the voltage representation $\begin{bmatrix} v_\alpha \\ v_\beta \end{bmatrix}$ in the αβ-frame reference prevailed by the application of Clark transformation to Eq. (1):

$$\begin{bmatrix} v_\alpha \\ v_\beta \end{bmatrix} = R_s \begin{bmatrix} i_\alpha \\ i_\beta \end{bmatrix} + \frac{d}{dt}\begin{bmatrix} \psi_\alpha \\ \psi_\beta \end{bmatrix} + \begin{bmatrix} e_\alpha \\ e_\beta \end{bmatrix} \tag{9}$$

with

$$\psi_\alpha = L_d i_\alpha - \psi_f \sin\theta,\ \psi_\beta = L_q i_\beta - \psi_f \cos\theta \tag{10}$$

In addition to the voltage representation, the PMSM mechanical dynamics are defined as:

$$J\frac{d\omega}{dt} + f_r\omega_r = T_e - T_l \tag{11}$$

3. ITSC Fault Detection Using a Hybrid T2-FL–EKF Approach

Building on the proven architecture of our previous work (Romdhane et al, 2023), the current method benefits from a technological upgrade through the integration of a T2-FL estimator. This estimator is dedicated to the adaptive estimation of stator resistance R_s, while the electrical and mechanical states of the motor are monitored by an EKF. This hybrid synergy leverages the uncertainty handling capabilities inherent to type 2 to optimise the overall accuracy of the diagnostic system.

The general conceptual model of the upgraded approach is presented in Figure 2. Precisely, the normalised values of the current error and its derivative are applied to the T2-FL inference system, and the resulting. ΔR_s is supplied to the EKF observer.

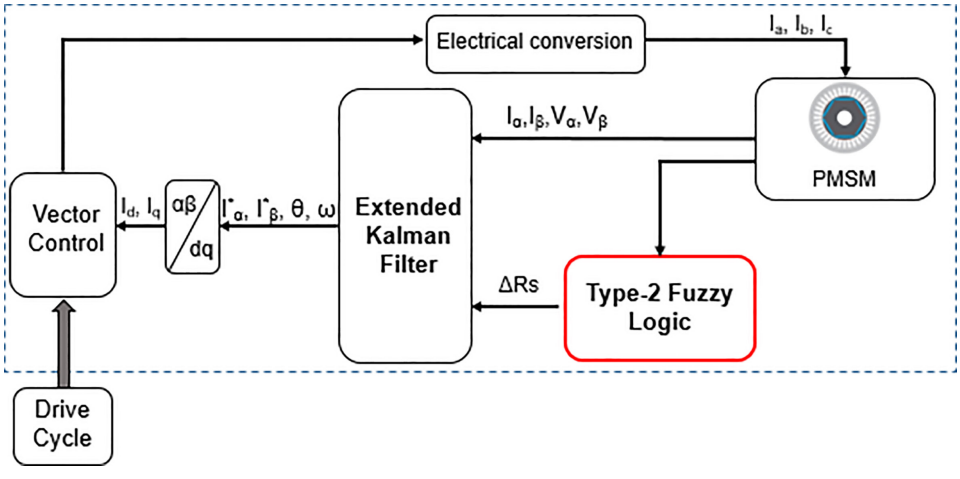

Figure 2. T2-FL–EKF conceptual model. PMSM, permanent magnet synchronous motor; T2-FL–EKF, type-2 fuzzy logic–extended Kalman filter.

The EKF then utilises the actual measures of the currents, voltages and the T2-FL estimator stator resistance to estimate the motor's internal states, namely the rotational speed, rotor angle and the stator currents (Baba and Cherkaoui, 2023). Contrasting the result values with the reference thresholds enables the detection of deviations that signal the emergence of winding ITSC.

3.1. Extended Kalman Filter modelling

The EKF adapts the conventional Kalman filter for use with non-linear systems. It provides recursive, real-time estimates of system states in the presence of measurement and process noise. The application of the first-order Taylor expansion in the approximation of the linearity function at the current state estimation helps the EKF to transform non-linear models into locally linearised forms described by their Jacobian matrices (Khodarahmi and Maihami, 2023).

Each update cycle consists of two fundamental stages: prediction, where the next state is forecasted using the system model, and correction, where this prediction is refined using newly acquired measurements (Kaniewski, 2020). The process iterates every sampling period T_s. The notion k signifies the moment after measurement updates, while k-1 indicates the moment before these updates occurred (Naoui et al., 2023).

The prediction process and update of the EKF are illustrated in Figure 3.

The initialisation stage is a crucial step where the state-space formulation of the EKF is expressed as follows:

$$\begin{cases} x(k+1) = g\left(x(k), u(k)\right) + \omega(k) \\ z(k) = h\left(x(k)\right) + v(k) \end{cases} \tag{12}$$

Where:

- $x(k)$: State matrix;
- $g(\cdot)$: Non-linear state-transition model;
- $z(k)$: Measurement matrix;
- $h(\cdot)$: Measurement function;
- $w(k)$, $v(k)$: The process and measurement zero-mean Gaussian noise vectors.

The second step is the prediction of the state, and the covariance of the predicted estimate is computed as follows:

$$P(k+1|k) = G(k)\, p(k) G(k)^T + Q \tag{13}$$

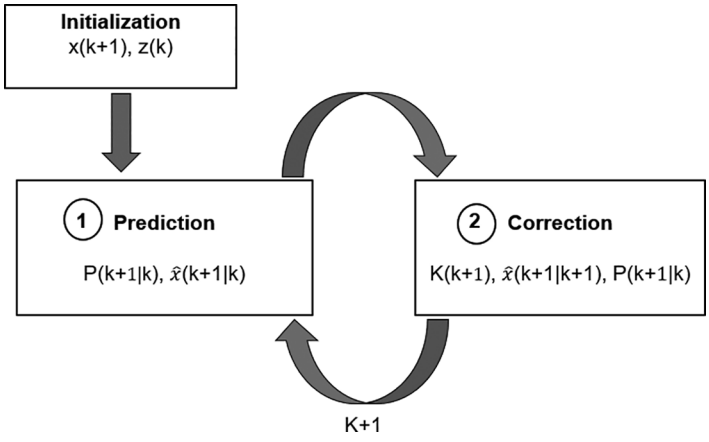

Figure 3. EKF flow diagram. EKF, extended Kalman filter.

Where:

Q is the covariance matrix of the process noise, while $G(k)$ is the Jacobian matrix represented by the following equation:

$$G(k) = \left.\frac{\partial g\left(x(k), u(k)\right)}{\partial x^T(k)}\right|_{x(k)=\hat{x}(k)} \tag{14}$$

When the measurement becomes available, the correction phase includes the updates beginning from the gain parameter $K(k+1)$ followed by the updated error covariance matrix update $P(k+1|k+1)$, which are calculated as follows:

$$K(k+1) = P(k+1|k)\left[H^T(k+1)P(k+1|k)H^T(k+1) + R\right]^{-1} \tag{15}$$

$$P(k+1|k+1) = \left[I - K(k+1)H(k+1)\right]P(k+1|k) \tag{16}$$

Where $h(k+1)$ is the Jacobian of $h(\cdot)$, and R represents the measurement noise covariance.

Finally, the estimated state vector is corrected according to:

$$\hat{x}(k+1|k+1) = \hat{x}(k+1|k) + K(k+1)\left[z(k+1) - h\left(\hat{x}(k+1|k)\right)\right] \tag{17}$$

3.2. EKF simulation model for the PMSM

A PMSM model formulation in the stationary α–β reference frame is preferred to ensure independence from position sensors. This choice helps to guard against rotor position initialisation errors, the impact of which could be detrimental to the accuracy of the EKF.

The state equation of the PMSM is given by the following equation:

$$\dot{x} = A(x,u) + B(u) \tag{18}$$

where: $x = [i\alpha, i\beta, \omega, \theta]^T$: State matrix, $u = [v\alpha, v\beta]$: Input matrix, and $y = [i\alpha, i\beta]^T$: Output matrix.

For transposition into the discrete frame time, Eq. (19) can be linearised as follows:

$$x_{k+1} = f(x_k, u_k) + \omega_k \tag{19}$$

where ω_k characterises the discrete noise vector.

3.3. T2-FL estimator for PMSM stator-resistance

As we mentioned previously, this proposed method is an enhancement of EKF's sensitivity for ITSC faults, by upgrading the stator resistance of the studied PMSM from FL to T2-FL, consistently with the same objectives of maintaining the best performance of the detection algorithm, in addition to conservation of the simplified implementation.

Figure 4 depicts the configuration of the type-2 fuzzy-based stator-resistance estimator (Dilmi et al., 2021).

3.3.1. FL principle

The inputs of the T2-FL estimator are E and E′, processed by a Mamdani inference pattern composed of 25 rules. The Karnik–Mendel algorithm, which is the crucial component, ensures the reduction used to estimate uncertainties before proceeding to the defuzzification phase using the centroid method. This principle is illustrated in Figure 5.

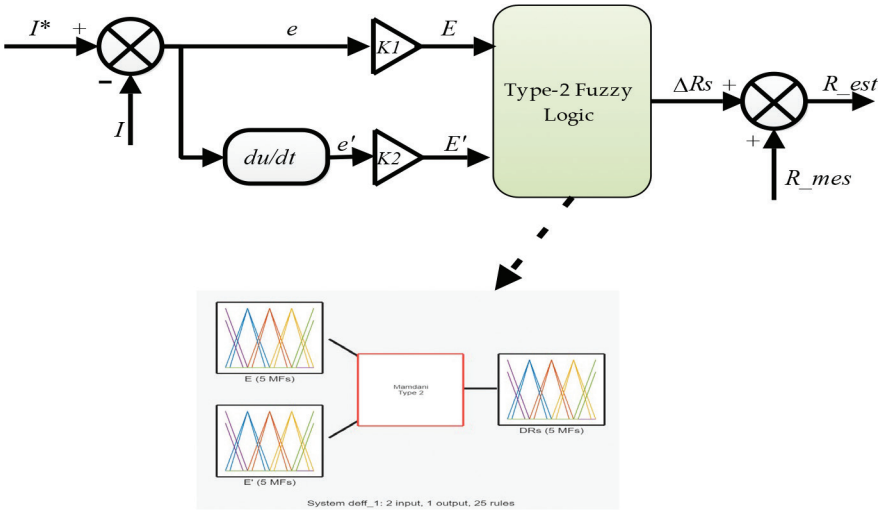

Figure 4. T2-FL estimator configuration. T2-FL, type-2 fuzzy logic.

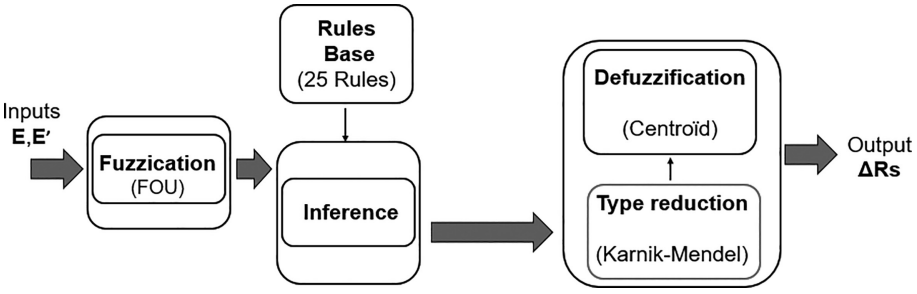

Figure 5. T2-FL estimator structure. T2-FL, type-2 fuzzy logic.

3.3.2. Fuzzy inputs and outputs

The estimator measures the stator current matrix error, characterised as the deviation of *I**, the estimated current and *I* relative to the reference *I*. It is expressed as follows:

$$\begin{cases} e = I^* - I \\ I^* = \sqrt{(i_\alpha^*)^2 + (i_\beta^*)^2} \\ I = \sqrt{i_\alpha^2 + i_\beta^2} \end{cases} \tag{20}$$

The inputs to the T2-FL system are the current error E and its derivative E', both normalised to lie within the interval [–1, 1]. The type-2 fuzzy output is the incremental adjustment amount in stator resistance (ΔR_s). The final stator resistance is then obtained through the recursive addition:

$$R_s(k+1) = R_s(k) + \Delta R_s(k) \tag{21}$$

As illustrated in Figure 6, the application of triangular membership functions enabled fuzzification of the exact input and output data into their respective T2-FL variables. In this investigation, the variables of the T2-FL estimator are resolved into three constituent levels.

3.3.3. Inference and rule base

The Mamdani-type inference mechanism is adopted due to its simplicity and interpretability. The type-2 fuzzy rule takes the following form: negative medium (NM), negative small (NS), zero (Z), positive small (PS) and positive medium (PM).

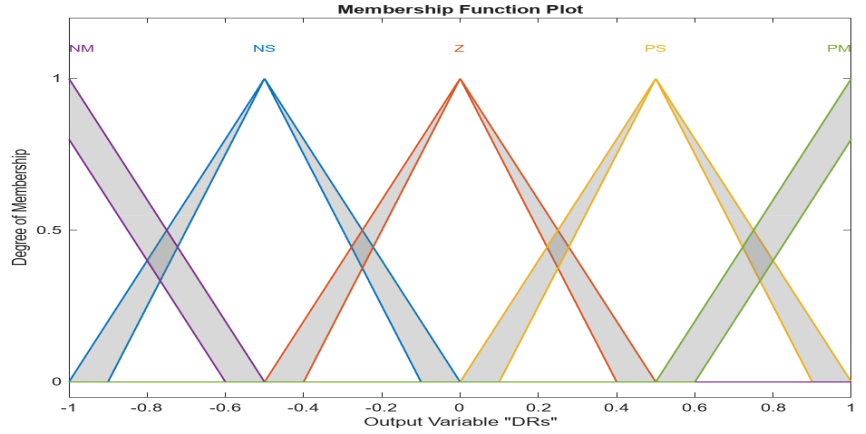

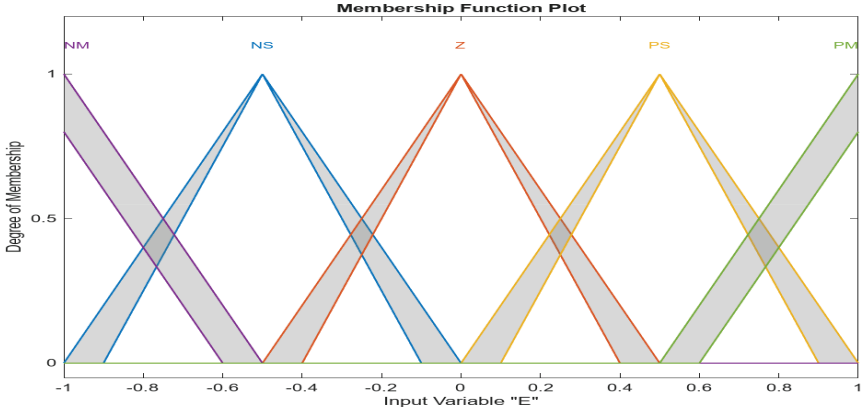

(a) Input Variable

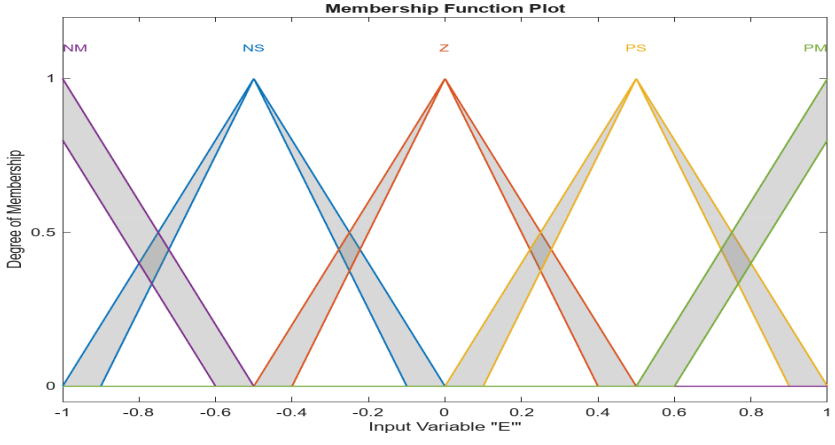

(b) Output Variable

Figure 6. T2-FL membership functions configuration. T2-FL, type-2 fuzzy logic. (a) Input variables and (b) Output variable.

Where *A*, *B* and *C* denote the linguistic variables.

A total of 25 rules (5 × 5) are defined, summarised in Table 1. The functional dependency of the current error on the stator resistance variation is recorded by this rule base.

As a type reducer, the Karnik–Mendel algorithm is the essential tool for transforming uncertainties into intervals of net values. It is an iterative algorithm known for its fast and guaranteed convergence. Subsequently, the defuzzification step is performed using Centroid to finally obtain the net value of the static resistance compensation.

4. Simulation Findings and Analysis

By leveraging MATLAB/SIMULINK tools for PMSM modelling and ITC fault detection with the upgraded version of FL–EKF to T2-FL–EKF, we were able to analyse the performance and test the robustness of our model. This section highlights the observations from this simulation.

4.1. Simulation set-up

During the simulation evaluation, the faulty condition is represented by $R_f = 1\,\Omega$ beside a variation of T_{fault}. The number of shorted turns in the sub-winding indicates the severity of the ITSC fault.

An application of a load torque of 1 N.m takes place in both the healthy and faulty states of the PMSM.

The two main objectives to be achieved in this simulation are the performance of the PMSM in terms of speed and control, and the sensitivity of ITSC detection under various conditions. Hence, the evaluation includes two tasks to examine:

- Robustness evaluation
- Sensitivity evaluation

4.2. Robustness evaluation

In order to evaluate the proposed approach, we opt to implement a reduced driving cycle starting with acceleration at $t = 0.1$ s to a speed of 160 rpm. Then, starting at 0.4 s, braking occurs, resulting in a deceleration until reaching 80 rpm. At 0.5 s, the engine rotation stops due to a second braking action, followed by acceleration to 120 rpm at $t = 0.8$ s. Finally, the rotational speed stabilises at 80 rpm until the end of the simulation.

This scenario represents a real-world driving experience with its various braking, acceleration and stopping states, which are typical in an urban area.

Figure 7 illustrates the temporal evolution of the PMSM speed obtained using the T2-FL–EKF method, compared with the actual measured speed. The results show excellent agreement between the two signals,

Table 1. T2-FL rule set for R_s determination.

E/E'	NM	NS	Z	PS	PM
NM	NM	NM	NS	Z	PS
NS	NM	NS	Z	PS	PM
Z	NS	Z	Z	Z	PS
PS	Z	PS	PS	PM	PM
PM	PS	PM	PM	PM	PM

NM, negative medium, NS, negative small, PM, positive medium, PS, positive small; T2-FL, type-2 fuzzy logic; Z, zero.

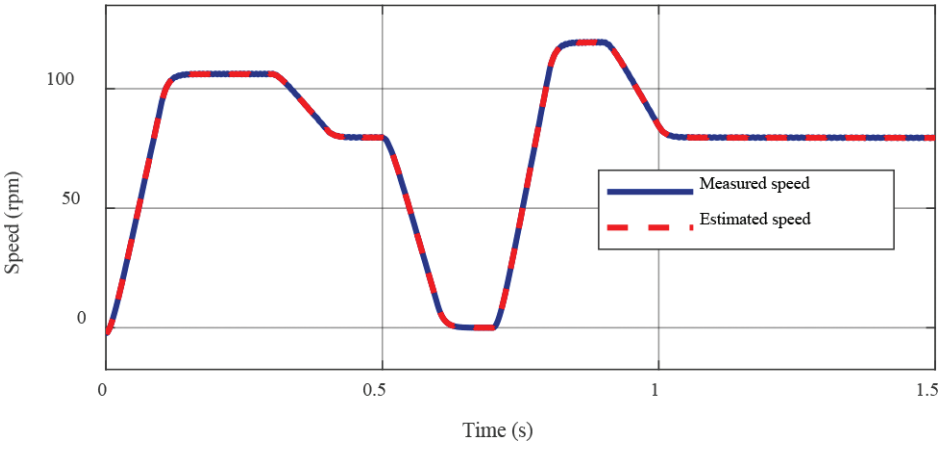

Figure 7. Dynamic speed regression.

demonstrating the high accuracy of the proposed speed observer. The small temporary differences observed during rapidly changing acceleration and deceleration conditions can be explained by the estimation model's response time and the effects of mechanical inertia. Under steady-state conditions, it was found to coincide with the measured speed, demonstrating the high accuracy and robustness of the T2-FL–EKF control strategy applied to the PMSM system.

In parallel with the development of speed, Figure 8 illustrates the reference driving cycle and the estimated angular velocity of the rotor (rad/s), giving a clearer view of how the estimator performs dynamically as expected. The comparison shows differences during sudden changes in the system due to the low delays of the observer in detecting rapid speed variations.

As shown in Figure 9, the estimated and measured angular positions are in acceptable agreement between the two signals. The curves follow the same model, showing that the estimation model is well synchronised with the actual motor.

These results demonstrate that the FL–EKF type II control provides an accurate estimate of the rotor position, which is required for effective vector control and sufficient synchronisation of stator and rotor.

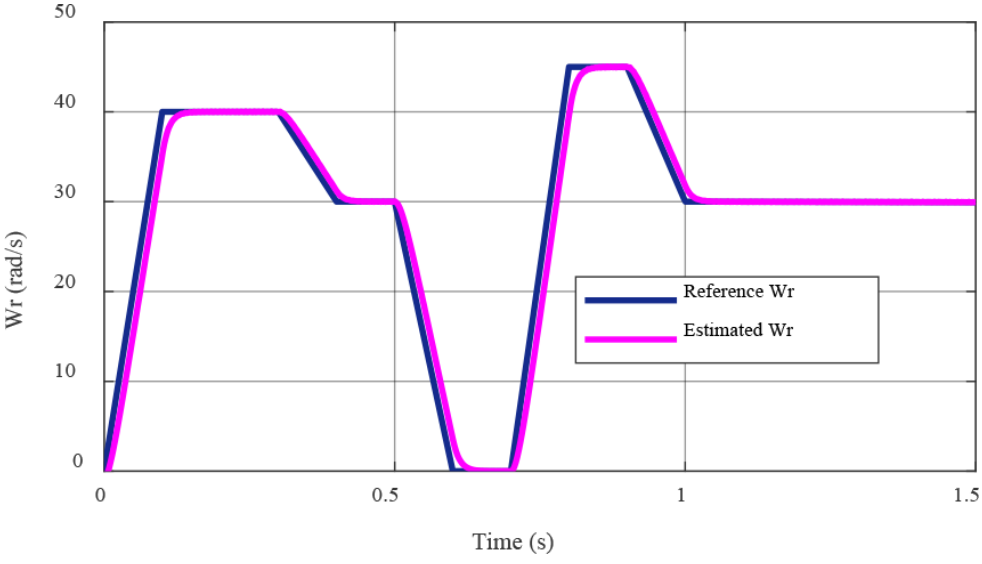

Figure 8. Rotor angular velocity.

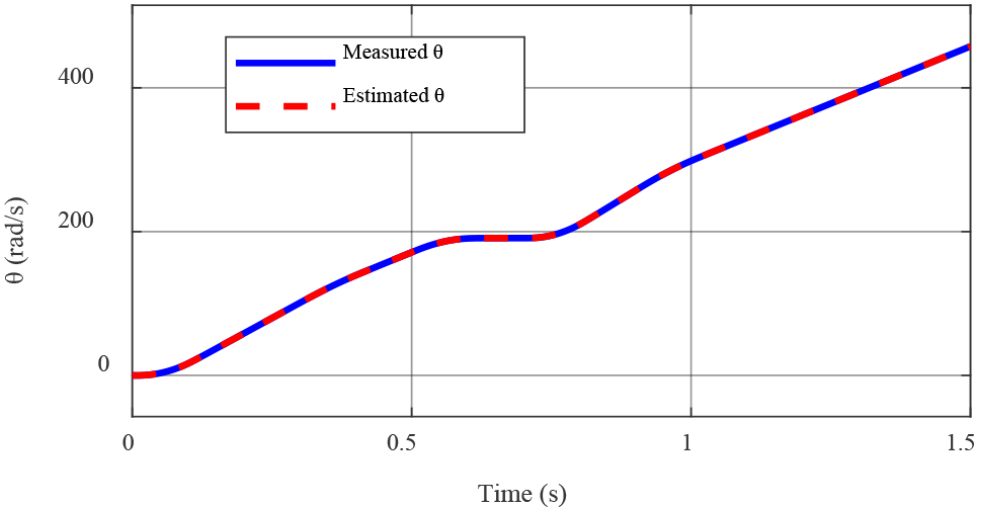

Figure 9. Angular position.

4.3. Sensitivity evaluation

This part concerns evaluation of the sensitivity of our upgraded approach to the detection of ITSC defects even in severe cases.

In fact, for this task R_f the fault resistance is set to 1 Ω, while we applied a variation in T_{fault} which implicates a variation in the ITSC fault severity. For the simulation, the ITSC fault appears at 0.8 s and its parameter variations are as indicated in Table 2.

The impact of a 50% ITSC fault, triggered at 0.8 s, is immediately identifiable by the asymmetry and instability of the current signals in Figure 10. Beyond transient fluctuations, ITSC faults can lead to mechanical vibrations and speed instabilities that are detrimental to ride quality. The persistence of such anomalies exacerbates thermal stresses on the windings, thus accelerating the motor's ageing process and compromising its operational reliability.

In Figure 11, the vector control currents evolution is carried out. At 0.8 s, increased ripples, rapid peaks and decaying oscillations can be observed in I_d and I_q currents. This reflects the perturbation of the electromagnetic torque. These anomalies in I_q directly translate into torque excursion and velocity variations, while alterations in I_d affect magnetic saturation and flux control accuracy.

Figure 12 illustrates the estimated and measured stator resistance, respectively, for μ = 25% and μ = 50%.

By calculating the root mean square error (RMSE), the T2-FL–EKF method shows a significant reduction in RMSE value as the fault coefficient μ decreases: the RMSE drops from 0.0076 when μ = 50% to 0.0052 when μ = 25%. This result reflects an increased ability of the proposed method to converge towards the real value despite the level of the disturbances induced by the ITSC fault.

Figure 13 shows the evolution of the estimated and measured fault current. Here, we proceeded to quantitatively evaluate the precision and accuracy of the T2-FL–EKF method.

Table 3 summarises the fault current value ($I_{f\,\text{moy}}$) determined at different fault levels, where the calculation of the RMSE.

The comparison of the estimated and measured average values $I_{f\,\text{moy}}$, shows that the two signals generally follow the same evaluation with a limited difference presented by RMSE.

Table 2. Indication of ITSC severity.

	μ (%)	T_{fault}	Severity	Indication
R_f = 1 Ω	μ = 25	40 turns	High	Poor visibility
	μ = 50	80 turns	Extremely high	Higher visibility

ITSC, inter-turn short circuit.

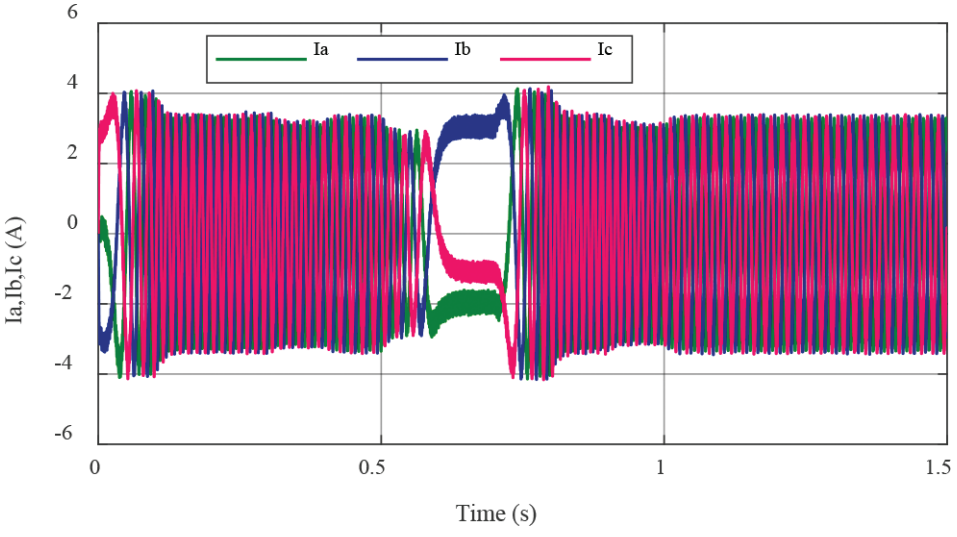

Figure 10. I_{abc} stator currents.

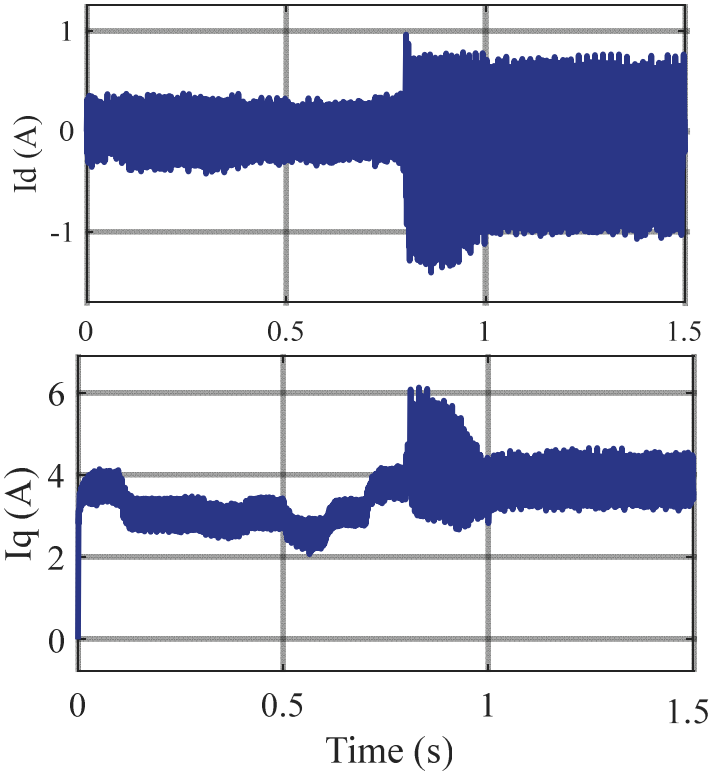

Figure 11. Vector control currents.

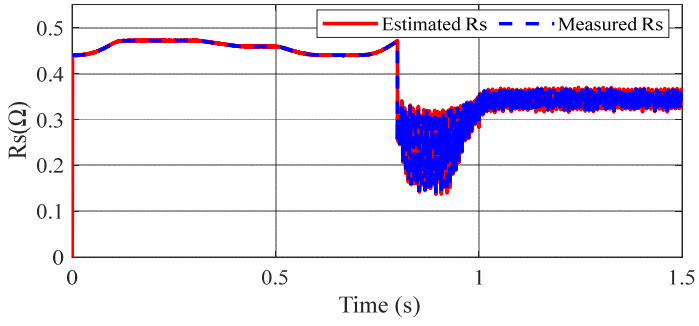

(a) $\mu = 25\%$

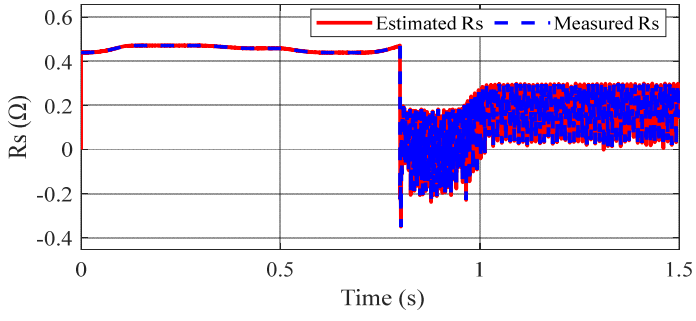

(b) $\mu = 50\%$

Figure 12. Stator resistance measurements. (a) $\mu = 25\%$ and (b) $\mu = 50\%$.

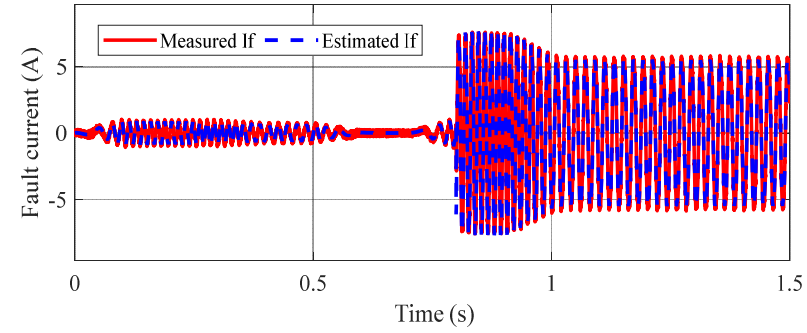

(a) μ = 25%

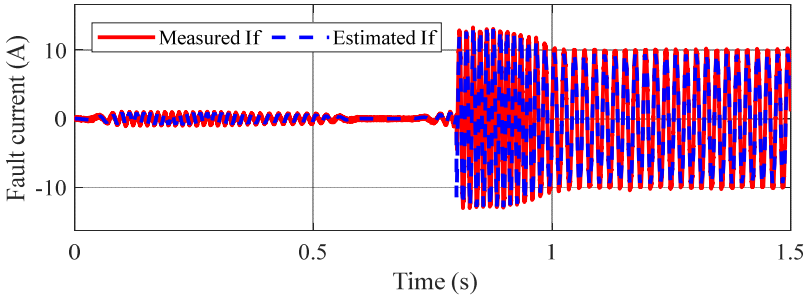

(b) μ = 50%

Figure 13. Fault current measurements. (a) μ = 25% and (b) μ = 50%.

Table 3. ITSC fault current values.

For R_f = 1 Ω	Estimated $I_{f\ moy}$	Measured $I_{f\ moy}$	RMSE
μ = 25%	0.0182	0.0216	0.2303
μ = 50%	0.0321	0.0416	0.5513

ITSC, inter-turn short circuit; RMSE, root mean square error.

For $\mu = 50\%$, the RMSE value is 0.05513, while for $\mu = 25\%$ it is 0.2303. This significant reduction confirms that the proposed method effectively extracts fault signatures, regardless of its severity level, and thus offers more precise and sensitive detection in situations where the fault remains weakly visible and thus hardest to detect.

4.4. Comparative analysis

To evaluate the proposed methodology (T2-FL–EKF) for ITSC fault detection, a comparative study was conducted with the classical EKF (Maanani and Menacer, 2019) and the hybrid EKF based on FL (Romdhane et al., 2023). In this study, and to ensure the validity of comparison, the three algorithms were evaluated within a unified framework. Each simulation, with a total time of 0.75 s, involved the application of an ITSC fault at time t = 0.2 s. The comparative evaluation of the algorithms was intentionally conducted under low fault visibility conditions (μ = 25%). After initial tests showed that ITSC fault detection was comparable for all algorithms at a 50% visibility level, it became necessary to focus on a more challenging scenario. The study at μ = 25% highlights the limitations of each algorithm and allows for a better assessment of its effectiveness under degraded conditions.

The comparison of the stator resistance R_s estimation precision of the three algorithms mentioned is presented in Figure 14. The EKF estimator observation in Figure 14a, shows large-amplitude fluctuations, although it is capable of tracking the stator resistance value. Without an intelligent compensation mechanism, the estimation remains subject to stochastic uncertainties. The integration of FL, as illustrated in Figure 14b, smooths the estimation. By acting as a smart filter, the fuzzy module absorbs some of the measurement noise. However, the fixed membership functions of Type 1 do not fully account for variable uncertainty. From Figure 14c, we conclude that the proposed

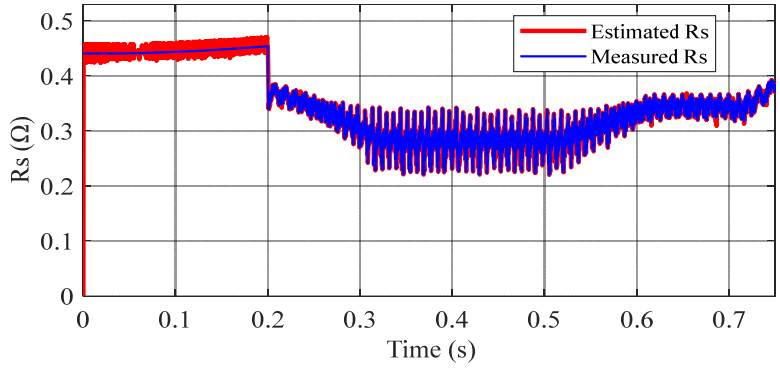

(a) EKF approach

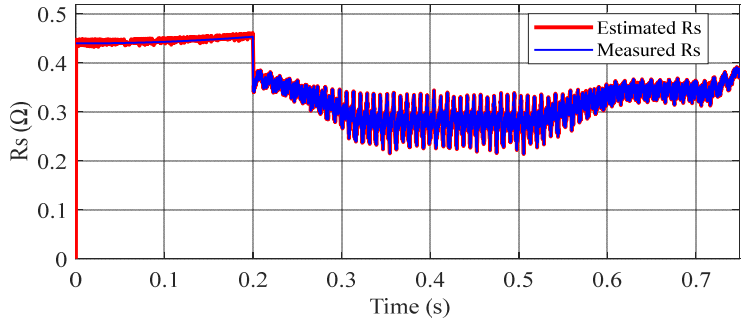

(b) FL EKF approach

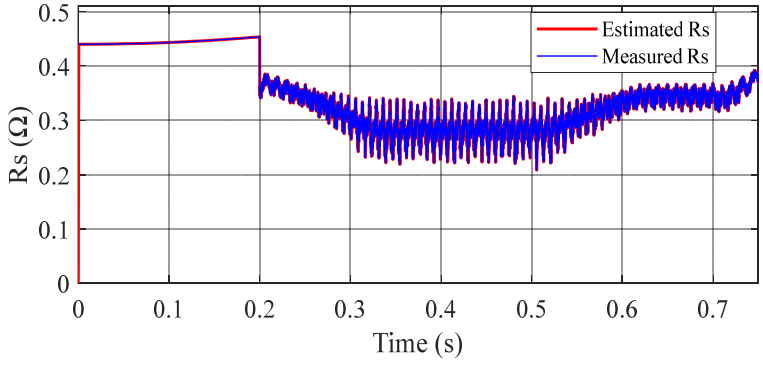

(c) T2-FL EKF approach

Figure 14. R_s estimation precision: (a) EKF approach, (b) FL–EKF approach and (c) T2-FL–EKF approach. T2-FL–EKF, type-2 fuzzy logic and extended Kalman filter; FL–EKF, fuzzy logic–extended Kalman filter.

approach T2-FL–EKF offers the most stable signal with a significant reduction in fluctuation amplitude. This performance is explained by the FOU, which allows the system to better tolerate inaccuracies in the EKF residuals, ensuring smooth convergence and increased accuracy in the stator resistance estimation.

The comparative analysis of the three approaches in Table 4, based on the RMSE and mean absolute percentage error (MAPE) indices, highlights the superiority of the T2-FL–EKF method.

Table 4. Summary of comparative techniques under the same simulation conditions.

Control strategy	RMSE of R_s estimation	MAPE of R_s estimation (%)	Estimation of R_s	Precision
EKF	0.010378	1.8435	Medium	Medium
FL–EKF	0.0066925	1.6348	High	High
Proposed optimised method	0.0066416	1.6101	High	Very high

EKF, extended Kalman filter; FL–EKF, fuzzy logic–extended Kalman filter; MAPE, mean absolute percentage error; RMSE, root mean square error.

The RMSE results reveal that the upgrade to the T2FL–EKF approach meets a minimum error of 0.0066416, representing a 36% improvement over the basic EKF method. This reduction demonstrates the system's ability to effectively stabilise the stator resistance estimation under high uncertainties. The MAPE analysis confirms this efficiency with a relative error of only 1.6101%.

Although the difference between the FL–EKF estimator and the T2-FL–EKF estimator appears small at the high-visibility level, the upgraded T2-FL–EKF approach offers superior robustness to non-linear variations, ensuring reliable diagnosis, especially in weakly visible ITSC faults where conventional methods might diverge.

Nevertheless, the high sensitivity of the proposed approach in ITSC fault detection for PMSM, even under low visibility of the fault, T2-FL–EKF has some limits. Mainly, the algorithm complexity compared with FL–EKF, regardless, is manageable by the main Karnik–Mendel algorithm. We can also find that the sensibility can be affected through footprint of uncertainty (FOU), and an inappropriate calibration can lead to an increase in the response time.

5. Conclusion

The hybrid T2-FLC–EKF method upgraded in this study represents a significant advance for the intelligent detection of electrical faults within PMSM motors for EVs. The use of the T2-FL structure for adaptive adjustment of stator resistance ensures high detection even in critical situations. The susceptibility of this method makes it possible to identify low-amplitude faults, often poorly visible for conventional methods, making the T2-FL–EKF solution a cutting-edge predictive maintenance tool for PMSM motors. Yet, this approach suffers from a higher computational load compared with conventional methods. The experimental validation will be carried out using a digital signal processor (DSP) acquisition card, serving as an interface between the MATLAB/SIMULINK environment and the power converter without the need for major restructuring of the algorithm.

Acknowledgements

There is no acknowledgement involved in this work.

Conflicts of Interest

The authors declare no conflicts of interest.

References

Amiri Ahouee, R. and Mola, M. (2020). Inter-Turn Fault Detection in PM Synchronous Motor by Neuro-Fuzzy Technique. *International Journal of System Assurance Engineering and Management*, 11(5), pp. 923–934. doi: 10.1007/s13198-020-01019-1

Arévalo, P., Ochoa-Correa, D. and Villa-Ávila, E. (2024). A Systematic Review on the Integration of Artificial Intelligence Into Energy Management Systems for Electric Vehicles: Recent Advances and Future Perspectives. *World Electric Vehicle Journal*, 15(8), p. 364. doi: 10.3390/wevj15080364

Baba, M. A., Naoui, M. and Cherkaoui, M. (2023). Modeling and Simulation of a BLDC Motor Speed Control in Electric Vehicles. *International Conference on Digital Technologies and Applications*, 1, pp. 883–895. doi: 10.1007/978-3-031-29857-8_88

Castillo, O., Amador-Angulo, L., Castro, J.R. and Garcia-Valdez, M. (2016). A Comparative Study of Type-1 Fuzzy Logic Systems, Interval Type-2 Fuzzy Logic Systems and Generalized Type-2 Fuzzy Logic Systems in Control Problems. *Information Sciences*, 354, pp. 257–274. doi: 10.1016/j.ins.2016.03.026

Cavus, M., Ayan, H., Bell, M. and Dissanayake, D. (2025). Advances in Energy Storage, AI Optimisation, and Cybersecurity for Electric Vehicle Grid Integration. *Energies (19961073)*, 18(17), p. 4599. doi. org/10.3390/ en18174599

De, A. K., Chakraborty, D. and Biswas, A. (2022). Literature Review on Type-2 Fuzzy Set Theory. *Soft Computing*, 26(18), pp. 9049–9068. doi: 10.1007/s00500-022-07304-4

Dilmi, I., Bouguerra, A., Djrioui, A. and Chrifi-Alaoui, L. (2021). Interval Type-2 Fuzzy Logic-Second Order Sliding Mode Based Fault Detection and Active Fault-Tolerant Control of Brushless DC Motor. *Journal Européen des Systèmes Automatisés*, 54, pp. 475–485. doi: 10.18280/jesa.540311

Ertargin, M., Yildirim, O. and Orhan, A. (2024). Mechanical and Electrical Faults Detection in Induction Motor Across Multiple Sensors With CNN-LSTM Deep Learning Model. *Electrical Engineering*, 106(6), pp. 6941–6951. doi: 10.1007/s00202-024-02420-w

Hang, J., Qiu, G., Hao, M. and Ding, S. (2024). Improved Fault Diagnosis Method for Permanent Magnet Synchronous Machine System Based on Lightweight Multi-Source Information Data Layer Fusion. *IEEE Transactions on Power Electronics*. 39(10), pp. 13808–13817. doi: 10.1109/TPEL.2024.3432163

Huang, B., Yu, W., Ma, M., Wei, X. and Wang, G. (2025). Artificial-Intelligence-Based Energy Management Strategies for Hybrid Electric Vehicles: A Comprehensive Review. *Energies*, 18(14), p. 3600. doi: 10.3390/en18143600

Isermann, R. (2004). Model-Based Fault Detection and Diagnosis-Status and Applications. *IFAC Proceedings Volumes*, 37(6), pp. 49–60. doi: 10.1016/s1474-6670(17)32149-3

Jahanshahi, H., Yousefpour, A., Soradi-Zeid, S. and Castillo, O. (2022). A Review on Design and Implementation of Type-2 Fuzzy Controllers. *Mathematical Methods in the Applied Sciences*, 49(3), pp. 1814–1835. doi.org/10.1002/mma.8492

Kaniewski, P. (2020). Extended Kalman Filter With Reduced Computational Demands for Systems With Non-Linear Measurement Models. *Sensors (Switzerland)*, 20(6), p. 1584. doi: 10.3390/s20061584

Khodarahmi, M. and Maihami, V. (2023). A Review on Kalman Filter Models. *Archives of Computational Methods in Engineering*, 30(1), pp. 727–747. doi: 10.1007/s11831-022-09815-7

Ladjal, B., Berrabah, F., Zeghlache, S., Djerioui, A. and FouadBenkhoris, M. (2022). Active Fault Tolerant Control Based on Backstepping Controller and Non Linear Adaptive Observer for Double Star Induction Machine. *International Journal of Intelligent Engineering and Systems*, 15(3), pp. 587–600. doi: 10.22266/ijies2022.0630.50

Lang, W., Hu, Y., Gong, C., Zhang, X., Xu, H. and Deng, J. (2022). Artificial Intelligence-Based Technique for Fault Detection and Diagnosis of EV Motors: A Review. *IEEE Transactions on Transportation Electrification*, 8(1), pp. 384–406. doi: 10.1109/TTE.2021.3110318

Lazar, A. E. N., Bendali, A. and Ferdjouni, A. (2021). ANN-approach for ITSC fault diagnosis of induction motor. In: *2021 IEEE Workshop on Electrical Machines Design, Control and Diagnosis (WEMDCD)*, Modena, Italy. pp. 231–236. doi: 10.1109/WEMDCD51469.2021.9425630

Liu, C., Xiao, L., Zou, J., Xu, Y. and Li, S. (2023). Analysis and Monitoring Method for Inter-Turn Short-Circuit Fault for PMSM. *IEEE Transactions on Magnetics*, 59(11), pp. 1–6. doi: 10.1109/TMAG.2023.3294704

Maanani, Y. and Menacer, A. (2019). Modeling and Diagnosis of the Inter-Turn Short Circuit Fault for the Sensorless Input-Output Linearization Control of the PMSM. *Periodica Polytechnica Electrical Engineering and Computer Science*, 63(3), pp. 159–168. doi: 10.3311/PPee.13658

Miller, T., Durlik, I., Kostecka, E., Borkowski, P. and Łobodzińska, A. (2024). A Critical AI View on Autonomous Vehicle Navigation: The Growing Danger. *Electronics*, 13(18), p. 3660. doi: 10.3390/electronics13183660

Namdar, A., Samet, H., Allahbakhshi, M., Tajdinian, M. and Ghanbari, T. (2022). A Robust Stator Inter-Turn Fault Detection in Induction Motor Utilizing Kalman Filter-Based Algorithm. *Measurement: Journal of the International Measurement Confederation*, 187(September 2021), p. 110181. doi: 10.1016/j.measurement.2021.110181

Naoui, M., Flah, A. and Sbita, L. (2023). Efficiency of Intelligent Control Design for Dual-Stator Machine on the EV Traction System. *Arabian Journal for Science and Engineering*, 48, pp. 15283–15304. doi: 10.1007/s13369-023-08070-7

Nesri, M., Nounou, K., Sifelislam, G., Benkhoris, M. F. and Azeddine, H. O. U. A. R. I. (2024). Hybrid Flatness-Based Control of Dual Star Induction Machine Drive System for More Electrical Aircraft. *EPE Journal-European Power Electronics and Drives*, 9(1), pp. 50–62. doi: 10.2478/pead-2024-0004

Nguyen, S. T., Pham, T. M., Hoang, A. and Cao, T.T. (2025). Optimal Tuning of Digital PID Controllers for Commercial BLDC Motors Using the Nelder–Mead Method. *Power Electronics and Drives*, 10, pp. 210–226. doi: 10.2478/pead-2025-0015

Nyanteh, Y. D., Srivastava, S. K., Edrington, C. S. and Cartes, D. A. (2013). Application of Artificial Intelligence to Stator Winding Fault Diagnosis in Permanent Magnet Synchronous Machines. *Electric Power Systems Research*, 103, pp. 201–213. doi: 10.1016/j.epsr.2013.05.018

Ouamara, D., Boukhnifer, M., Chaibet, A. and Maidi, A. (2023). Diagnosis of ITSC Fault in the Electrical Vehicle Powertrain System Through Signal Processing Analysis. *Diagnostyka*, 24(1), pp. 2449–5220. doi: 10.29354/diag/161309

Prakash, Z. (2025). Integration of AI and ML in Regenerative Braking for Electric Vehicles: A Review. *Frontiers in Artificial Intelligence*, 8, p. 1626804. doi: 10.3389/frai.2025.1626804

Romdhane, M., Naoui, M. and Mansouri, A. (2023). PMSM Inter-Turn Short Circuit Fault Detection Using the Fuzzy-Extended Kalman Filter in Electric Vehicles. *Electronics*, 12(18), p. 3758. doi: 10.3390/electronics12183758

Sanchez, M. A., Castillo, O. and Castro, J. R. (2015). Generalized Type-2 Fuzzy Systems for Controlling a Mobile Robot and a Performance Comparison With Interval Type-2 and Type-1 Fuzzy Systems. *Expert Systems with Applications*, 42(14), pp. 5904–5914. doi: 10.1016/j.eswa.2015.03.024

Shao, S., Yan, R., Lu, Y., Wang, P. and Gao, R. X. (2020). DCNN-Based Multi-Signal Induction Motor Fault Diagnosis. *IEEE Transactions on Instrumentation and Measurement*, 69(6), pp. 2658–2669. doi: 10.1109/TIM.2019.2925247

Tan, K., Wu, J., Zhou, H., Wang, Y. and Chen, J. (2024). Integrating Advanced Computer Vision and AI Algorithms for Autonomous Driving Systems. *Journal of Theory and Practice of Engineering Science*, 4(1), pp. 41–48.

Yu, H., Li, S., Xu, Y., Zhang, Z., Mu, H. and Han, W. (2025). Time-Frequency Domain Lightweight Dual-Branch MSCFormer for PMSM ITSC Fault Diagnosis. *IEEE Transactions on Industrial Electronics*, 73(1), pp. 94–105. doi: 10.1109/TIE.2025.3579108

Zeng, Y., Hussein, Z. A., Chyad, M. H., Farhadi, A., Yu, J. and Rahbarimagham, H. (2025). Integrating Type-2 Fuzzy Logic Controllers With Digital Twin and Neural Networks for Advanced Hydropower System Management. *Scientific Reports*, 15(1), p. 5140. doi: 10.1038/s41598-025-89866-5

Zhang, W., Xu, Q., Gao, L., Miao, Y., Cai, H. and Zhao, Y. (2025). ITSC Fault Diagnosis for PMSM by Using Adaptive Filtering and Tree-Structured Parzen Estimator Optimized-Automated Random Forest. *Electrical Engineering*, 107(4), pp. 4711–4725. doi: 10.1007/s00202-024-02788-9